Volume 14, Issue 3, 142425 (1-16)

Iranian Journal of Catalysis (IJC)

https://doi.org/10.57647/j.ijc.2024.1403.25

Efficient photocatalytic esterification of waste cooking oil over empty fruit bunches ash-supported TiO_2

Siti Fadhilah Ibrahim[1], Norshahidatul Akmar Mohd Shohaimi[1,2*], Zul Adlan Mohd Hir[1], Mohd Sufri Mastuli[3], Taufiq Yap Yun Hin [4], Mohd Lokman Ibrahim[3]

[1]*Faculty of Applied Sciences, University Technology MARA Pahang, Bandar Tun Abdul Razak Jengka, Pahang, Malaysia.*
[2]*Advanced Biomaterials and Carbon Development Research Group, Faculty of Applied Sciences, University Technology MARA, Shah Alam, Selangor, Malaysia.*
[3]*School of Chemistry and Environment, Faculty of Applied Sciences, University Technology MARA, Shah Alam, Selangor, Malaysia.*
[4]*Catalysis Science and Technology Research Centre (PutraCAT); Faculty of Science, University Putra Malaysia, UPM Serdang, Selangor, Malaysia,*

*Corresponding authors: akmarshohaimi@uitm.edu.my

Original Research

Received:
31 March 2024
Revised:
14 May 2024
Accepted:
14 June 2024
Published online:
1 July 2024

Abstract:

Biodiesel production from waste cooking oil (WCO) holds promise as a renewable and sustainable energy source. However, high levels of free fatty acids (FFAs) in WCO require efficient pre-treatment before transesterification. Utilizing solar energy for heterogeneous catalytic reactions offers an alternative to thermal-driven processes. TiO_2EFBA, synthesized via the wet impregnation method, exhibits distinctive physicochemical properties confirming the successful incorporation of titanium dioxide (TiO_2) onto the metal oxides of empty fruit bunches ash (EFBA), thereby enhancing the catalyst's performance and stability. Results showed that TiO_2EFBA exhibits superior FFA conversion compared to TiO_2 alone. Under optimized reaction conditions, employing 4 wt% TiO_2EFBA catalyst, 20:1 methanol to oil molar ratio, and 2 h reaction time at room temperature under Ultra Violet (UV) light, achieves a remarkable 78% conversion rate of FFAs in WCO. Mechanistic investigation reveals the crucial role of electron/hole (e^-/h^+) species in reducing FFAs by suppressing the e^-/h^+ mechanism. Notably, TiO_2EFBA facilitates easy separation and can be reused for 10 cycles, demonstrating its stability as a heterogeneous photocatalyst.

Keywords: Biodiesel; Empty fruit bunches ash; Metal oxide; Photo-esterification; Photo-catalyst; Waste cooking oil

1. Introduction

In 2024, the global production of liquid fuels is expected to surge by 1.0 million barrels per day (b/d), a projection highlighted by the International Energy Agency (IEA). This increase in production, coupled with soaring demand, may exert upward pressure on crude oil prices in the forthcoming year. Projections suggest a rise from the current average of $90 per barrel (b) to an anticipated average of $93/b in 2024 [1]. Consequently, the escalating depletion of petroleum-based fuels has spurred intensive research into viable alternatives that are both renewable and environmentally friendly. One promising substitute is biodiesel, scientifically known as fatty acid methyl ester (FAME), which is derived from plant oils or animal fats. It stands out as a superior alternative to traditional petroleum diesel, boasting qualities such as being clean-burning, non-toxic, renewable, and sustainable [2]. Several factors influence the production cost of biodiesel, as elucidated by Chozhavendhan et al., including the choice of feedstock oil, catalyst, and methanol [3]. The use of vegetable oil, although environmentally friendly, may prove more costly than petroleum-based fuels

due to its limited availability and competition with crop production [4]. Additionally, employing non-edible feedstock oil presents challenges, such as the saponification problem arising from FFAs and water content [5]. However, the production of biodiesel using non-edible feedstock oil can offset production costs, yielding a product that complies with the stringent international standard ASTM D-6751 for biodiesel. As the world seeks sustainable energy alternatives, biodiesel emerges as a promising candidate, combining environmental benefits with the potential to meet global energy demands [6].

In Malaysia, WCO primarily originates from food frying and is sourced from palm oil refineries. Generally comprising triglycerides, which are glycerol esters of fatty acids, WCO exhibits physicochemical properties and compositions distinct from vegetable oil or fresh cooking oil due to oxidation and thermal decomposition resulting from frying temperature and cooking duration. The generation of WCO accounts for 20 – 30% of the total from fresh palm oil and its quantity can be computed using the formula as per equation 1 [7]. With a current population of 34 million in Malaysia and a per capita oil palm consumption of 3.3 million metric tons based on 2022 data, the nationwide production of WCO amounts to 22.44 million kg. Improper disposal of WCO poses a threat to sewage pipelines, leading to environmental pollution that adversely affects flora and fauna. Given its ready availability and lower cost compared to palm oil, WCO can serve as a practical substitute for feedstock oil in biodiesel production. WCO is enriched with monoglycerides, diglycerides, and FFA due to the hydrolysis process during food preparation. The utilization of WCO in biodiesel production offers a novel avenue characterized by lower activation energy, simultaneously addressing the challenge of oil disposal [8].

$$\text{WCO production} = \text{Population} \times \text{Oil Consumption Per Capital} \times 20\% \quad (1)$$

Wong et al. employed a homogeneous acid catalyst in the initial step of the esterification process, referred to as the pre-treatment process, to reduce the percentage of FFAs [9]. However, this approach proves to be expensive, needs high temperatures, and suffers from the drawback of non-reusable catalysts, leading to substantial water waste. In contrast, recent advancements in solar-driven photocatalysis have demonstrated a reduction of over 90% in FFAs content in low-cost feedstock oil [10]. This approach operates at room temperature and harnesses light energy as the driving force for efficiency and environmental friendliness compared to thermal catalytic reactions. When light strikes the surface of the photocatalyst, the photoelectric effect occurs, leading to the excitation of electron (e^-) from the valence band (VB) to the conduction band (CB), creating a hole (h^+) in the VB [11, 12]. The generation of e^-/h^+ initiates redox reactions with Reactive Oxygen Species (ROS) adsorbed on the catalyst surface. Dhull et al. have highlighted the crucial role of ROS in enhancing photocatalytic activity. ROS molecules, including hydroxyl radicals (•OH), superoxide radicals ($\bullet O_{2-}$), hydrogen peroxide (H_2O_2), singlet oxygen ($^1O_2$), and others, are generally involved in pollutant degradation, cellular damage, and water purification [13, 14]. According to Corro et al., during photo-esterification, photoinduced e^-/h^+ pairs react with FFAs and methanol on the catalyst surface, generating radical species such as methanol radical ($CH_3O\bullet$), FFAs radical ($RCO\bullet$)OH, and hydrogen ions (H^+) [15]. This initiates a chemical reaction and restores electrical neutrality through e^-/h^+ recombination. These radical species undergo an intermediate process, ultimately producing the desired ester product [16, 17]. As reported by Younis et al., photocatalysis boasts several advantages, including its ability to catalyze multiple redox reactions per active site, which can produce a high yield of FAME [18].

In 1972, Fujishima and Honda first introduced TiO_2 in the photolysis of water under UV light irradiation [19]. Since then, a diverse range of semiconductor photocatalysts has been developed for various photocatalytic applications. TiO_2 is particularly noteworthy due to its semiconductor efficiency, offering good chemical and mechanical stability, affordability, high reactivity, excellent redox selectivity, and non-toxic properties [20]. However, its wide bandgap energy (∼3.0-3.5 eV) and the limitation of operation primarily under UV-light conditions (∼5% of sunlight) rather than visible light (∼40% of sunlight) can restrict its applicability[21]. Additionally, TiO_2 exhibits high e^-/h^+ recombination rates and low surface area, complicating target molecule adsorption [22]. Several techniques, such as doping, co-doping and composites methods, have been explored to address the issues that can modify the semiconductor's band structure [23, 24]. For instance, doping introduces metal or non-metal elements into TiO_2 , which creating trap states for charge carriers and reducing the recombination [25, 26]. Modification of TiO_2 with metal oxides has shown promise in enhancing photocatalytic performance. Examples include SO_4^{2-}/Au-TiO_2 [27], TiO_2/RGO [28], and Fly-ash/TiO_2 [29]. One study utilized TiO_2 doped with La^{3+} and ZnO in photo-esterification reporting to improve catalyst performance by reducing the bandgap width and e^-/h^+ recombination [30]. Another study focused on modifying TiO_2 nanotubes, finding that the modification increases the surface area and crystallinity, enhancing the adsorption process and catalyst stability [10]. By altering the surface and structural properties of the photocatalyst, the recombination rate, and charge carrier separation can be improved, and increasing carrier mobility.

The study focuses on using ash material containing various metal oxide such as K_2O, SiO_2, CaO, SO_3, MgO, P_2O_5, Al_2O_3, and Fe_2O_3 to modify the bandgap energy of semiconductor TiO_2 catalyst. Deposition of TiO_2 onto porous supported matrices like EFBA alters energy level, surface characteristics, and bandgap energy, preventing aggregation and providing insight into TiO_2EFBA mechanisms during integration and esterification [31]. These metal oxides can be integrated as a dielectric layer in a TiO_2 semiconductor, distorting its crystal lattice and altering its surface characteristics [32–34]. Dhull et al. reported that the interaction of TiO_2 with metal oxide in ash material could form heterojunctions or interfaces, enhancing charge separation and transfer process [11].

The aim of this research is to explore a novel approach for pretreating WCO through a photo-esterification process. This method is designed to convert low-quality feedstock oil using solar light irradiation at room temperature. The process is catalyzed by a heterogeneous semiconductor photo-catalyst, which can be reused multiple times while maintaining stability and catalytic efficacy. Furthermore, the study aims to develop a photocatalyst by incorporating TiO_2 with EFBA using varying mass ratios through the water-based-wet impregnation method. This approach allows for the incorporation of specific functional group into the catalyst structure, enabling tailored catalytic activity. Additionally, it promotes better dispersion and uniform impregnation. This method promotes cost effectiveness, aligning with green chemistry and sustainability goals [35]. Detailed analysis includes the catalyst's light absorption capabilities under various light intensities and its application in photo-esterification to improve carrier separation and promote interface reactions. Optimization involves determining the TiO_2EFBA mass ratio, reaction conditions, and catalyst loading for efficient biodiesel production.

2. Experimental

2.1 Materials

All the chemicals, absolute methanol (CH_3OH) (HmbG chemicals brand), isopropanol (R & M chemicals brand) analytical reagent (AR), toluene, 98% (QReC brand), hydrochloric acid (HCl) (37%) and titanium dioxide (TiO_2), phenolphthalein pH indicator solution (UNI-CHEM brand) were purchased from BT Science Sdn. Bhd (Selangor, Malaysia). Potassium hydroxide (KOH) pellet and sodium hydroxide (NaOH), the standard of methyl heptadecanoate, and n-hexane (99%) were purchased from Sigma-Aldrich (M) Sdn. Bhd. The chemicals were used as received without undergoing additional purification processes. Bhd (Malaysia). EFBA was acquired from FTJ Bio Power Sdn. Bhd. EFBA was dried in an oven at 100°C, and sieved using 100 mesh sizing to get a smaller size. WCO was collected from a public restaurant located in Bandar Jengka Pusat, Pahang, Malaysia. WCO was filtered to remove unnecessary particles and heat at 100°C for 5 to 10 min to remove moisture content. The acid value and saponification value test of WCO were determined using the titration method followed (AOCS; Cd 3a-63) standard and ASTM D5558, respectively, to calculate the FFA value and molecular weight of WCO using equations 2 until 5. The fatty acid properties of the WCO are listed in Table 1.

$$\text{Acid Value, AV } (\text{mgKOHg}^{-1}) = [(\text{V - B}) \times \text{C} \times 56.11]/\text{m} \quad (2)$$

where V is the volume of isopropanol KOH consumed to reach the titration end-point (mL), b is the volume of the blank test without sample product (mL), C is the concentration of KOH standard solution (0.1 N), 56.11 is the molecular weight of KOH and m is the mass of test sample (g).

$$\text{Free Fatty Acid, FFA}(\text{wt}(\%)) = \text{AV}/2 \quad (3)$$

$$\text{Saponification value, SV}(\text{mgKOHg}^{-1}) = [(\text{B - S}) \times \text{N} \times 56.11]/\text{W} \quad (4)$$

where B is the 0.5 N HCl solution required for titration of the blank (mL), S is the 0.5 N HCl solution required for the titration of the sample (mL), N is the normality of isopropanol KOH, 56.1 is the molecular weight of KOH and W is the weight of the sample (g).

$$\text{Molecular Weight } (\text{gmol}^{-1}) = (56.11 \times 3 \times 1000)/\text{SV} \quad (5)$$

where SV is the saponification value (mgKOHg^{-1}).

2.2 Catalyst preparation

TiO_2EFBA photocatalyst were prepared using the wet impregnation method. In this process, TiO_2 powder (85% rutile and 15% anatase) was mixed with EFBA employing various mass ratios in gram (x-TiO_2; y-EFBA) (1x:1y, 1x:2y, 1x:3y, 2x:1y, 3x:1y). The powder mixture of TiO_2 and EFBA was immersed in 100 mL deionized water and stirred for 1 h at room temperature. The mixture was then filtered and washed with deionized water. The slurry was dried in an oven at 100°C for 8 h. The resulting solid material was labeled as xTiO_2/yEFBA, where x represents the TiO_2 mass ratio, and y represents the EFBA mass ratio.

2.3 Catalyst characterization

The crystalline phase structure of the photocatalyst was examined using an X-ray diffractometer (LabX XRD-6000, Shimadzu) with Cu-Kα radiation (λ = 0.15406 nm, 15 mA). The scanning range spanned from 20 to 80°, with a scan rate of $2^\circ/\text{min}^{-1}$, and operated at 30 kV. The morphologies of the photocatalyst were observed through a scanning electron microscope (SEM, TESCAN VEGA3) at an accelerating voltage of 15 kV. Surface elemental composition was identified using Energy-Dispersive X-ray (Oxford instruments, X-Max^N) analysis. Chemical changes in the photocatalyst were analyzed using the Fourier-Transform Infrared Spectroscopy (FT-IR) technique. The FT-IR spectra were recorded using an FT-IR Spectrum 100 instrument (Perkin Elmer) in the wavelength range of 400–4000 nm, employing Perkin Elmer ATR. To determine the optical band gap (E_g) of the samples, the reflectance of photocatalyst was conducted using a PerkinElmer UV-VIS-NIR (Lambda 950) spectrophotometers. The UV Winlab software was used to analyze the sample edge of the sample. Wavelength Dispersive X-ray fluorescence (WD-XRF) has been used to analyze the element rate of the photocatalyst after the reusability test to determine leaching of the catalyst. This analysis was conducted using Rigaku/ZSX Primus II.

Table 1. Properties of WCO.

Properties	WCO
Acid value (mg KOH g^{-1})	24.8
Free Fatty Acid (wt.%)	12.4
Saponification value (mg KOH g^{-1})	183.9
Molecular weight (gmol^{-1})	914.9
Moisture content (%)	0.5

2.4 Pre-treatment WCO (photo-esterification)

The TiO_2EFBA catalyst was screening first on reaction parameter which are reaction time, methanol to oil molar ratio and catalyst loading under UV light with long wave (365 nm). The optimized condition will then be used to screen the activity and performance of the catalyst which are mass ratio of catalyst and type of lamp. Then, the reusability and scavenger test to determine the stability of catalyst and mechanism of the reaction.

The photo-esterification of WCO was first performed in a closed box equipped with a magnetic stirrer plate and a UV lamp 365 nm (6 watt). The TiO_2EFBA photocatalyst was investigated by evaluating its catalytic activity in the esterification of WCO. The optimized parameters included reaction times in the range of (1 h, 2 h, 3 h, 4 h, and 5 h), methanol-to-oil molar ratios (12:1, 16:1, 20:1, and 24:1), and catalyst loadings (1 wt%, 2 wt%, 3 wt%, 4 wt%, and 5 wt%). The reaction mixture was put into a 100 mL bottle sample of glass Duran. TiO_2EFBA catalyst was dispersed in a mixture of WCO and closed it tightly to avoid evaporation of methanol during the reaction process. UV light is irradiated during the reaction process, and continuous stirring is used to enhance the transfer rate of reactants and products at the interface of the catalyst and liquid phase. Once the reaction was complete, the reaction mixture was transferred to a centrifuge tube and centrifuged at 4000 rpm for 15 minutes to separate the solid and liquid products. The liquid product was then heated at 60°C for 10 minutes to remove excess methanol. Then, the FFA value was determined using the titration method (AOCS; Cd 3a-63), and calculated the FFA conversion using the equation 6. The optimized reaction parameter was then applied in the next photo-esterification using various mass ratio of TiO_2EFBA, and the last one was different light intensity which are without light sources, under UV lamp 254 nm (6 watt), visible lamps (23 watt) and xenon lamp (250 nm) to determine the photocatalytic performance using different light intensity.

$$\text{FFA conversion}(\%) = ([A_a - A_b]/A_a) \times 100 \quad (6)$$

where A_a is the acid value of WCO and A_b is the acid value of esterified WCO after photo-esterification reaction.

2.5 Transesterification

The esterified WCO was subjected to a transesterification reaction using the conventional reflux method. The Transesterification reaction was carried out on a laboratory scale in a 250 mL two-neck round bottom flask equipped with a water-cooled condenser and a constant temperature magnetic stirrer hotplate also thermometer to check the temperature of the reaction. The reaction mixture was then vigorously stirred and refluxed at 65 °C for 1 h, utilizing a 1 wt% sodium hydroxide (NaOH) catalyst and 12:1 methanol to esterified WCO with 5 g of esterified WCO under 400 rpm. After completing the reaction, the mixture was then separated using a separating funnel to separate the glycerol from the liquid product (FAME). The mixture was allowed to settle for 15 min and the complete settling can take as long as 24 h. After complete separation, the dark brown of glycerol at the bottomed of the separating funnel was removed. The non-polar product composed of FAME and solvent was washed with hot distilled water (> 80°C) to remove the catalyst, soap residue, and other contaminants. FAME product was weighed after the washing step to be used in the calculation formula of yield FAME using Gas Chromatography-Mass Spectrometry (GCMS) analysis.

2.6 Biodiesel characterization

The FAME composition and yield percentage were analyzed using GCMS analysis, specifically the Agilent Technologies GC system (7890 B) equipped with a mass spectrometer (MSD; 5977A). The non-polar capillary GC column (Phase: Zebron ZB-FAME) with dimensions were as follows: length (L) of 60 mm, inner diameter (ID) of 0.25 mm, and film thickness (FT) of 0.20 μm. Helium was used as carrier gas with 0.9 mL/min. The oven program was set for three steps: initial temperature at 40 °C holding for 1 minute, increasing to 180 °C at a rate of 5 °C/min, holding for 2 minutes, and increasing to 250 °C at a rate of 5 °C/min, holding for 2 minutes. For sample preparation, 0.125 g of FAME product was dissolved in 10 mL n-hexane (99%) and 10 mg/mL of internal standard (methyl heptadecanoate). 1 μL of the sample was then injected into the injection port septa of GC with a spitless ratio. The injector temperature was set at 80 °C and the interface at 260 °C. Ester content was quantified according to EN 14103 in the presence of methyl heptadecanoate as the internal standard. The final FAME yield product was calculated using the following equations 7 until 9.

$$\text{Ester content, c}\ (\%) = ([\text{TA-AEI}]/\text{AEI}) \times ((\text{CEI} \times \text{VEI})/\text{m}) \times 100 \quad (7)$$

where TA is the total area of methyl ester from GCMS analysis, AEI is the area of internal standard (methyl heptadecanoate) from GCMS analysis, CEI is the concentration of the internal standard (mgmL^{-1}), VEI is the volume of internal standard, and m (mg) is mass of sample that mixed with internal standard.

$$\text{Mass of pure biodiesel, Y (g)} = (\text{c}/100) \times \text{d} \quad (8)$$

where c is the ester content and d is the mass of FAME after transesterification.

$$\text{FAME yield}(\%) = (\text{Y/mass of oil}) \times 100 \quad (9)$$

where Y is the mass of pure biodiesel from the GCMS yield calculation, and the mass of oil is the mass of the sample before transesterification (mass of esterified oil).

2.7 Reusability test

The reusability test of the catalyst was carried out to study the stability of the TiO_2EFBA. The catalyst from each cycle was recovered by simple washing with hexane until the catalyst was removed from the residue of WCO that stick to the catalyst. The washing step was done using a centrifuge for multiple times. The catalyst was then filtered and dried in the oven for 10 to 15 min at 70 °C to remove excess hexane. The catalyst was reused for the next photo-esterification using optimized reaction conditions and then was rewashed and reused again for the next cycle. The leaching test was done using XRF analysis.

2.8 Scavenger Test

The scavenger test is employed to explore the reactive species in the TiO_2EFBA photocatalyst responsible for the esterification of WCO. Various scavenger tests will be conducted using ethylenediaminetetraacetic acid (EDTA), p-Benzoquinone (P-BQ), isopropanol alcohol (IPA), and Silver Nitrate ($AgNO_3$) to investigate the active species involvement in the reaction. This experiment involves the addition of 2 ml of 0.1 M scavenging solution under optimized reaction parameters. The FFA value results will be determined using the AOCS; Cd 3a-63 titration method and calculated using Equations 2 and 3.

3. Results and discussion

3.1 XRD analysis

XRD analysis is to determine the crystal phase, crystallinity and crystal size of the nanocomposite materials. The XRD pattern of EFBA, TiO_2, and various mass ratios of TiO_2EFBA, $3TiO_2$EFBA, $2TiO_2$EFBA, TiO_2EFBA, $TiO_2$2EFBA, and $TiO_2$3EFBA, was presented in Fig. 1. The composition of EFBA is attributed of metal oxides which serve as catalytic support for TiO_2. The identification of these phases was done by comparing them with the Joint Committee for Powder Diffraction Standard (JCPDS) cards. The identified peaks located at $2\theta = 28.20°$ and $40.97°$ are correspond to quartz (2 1 1) and (2 1 0) plane diffraction, respectively (JCPDS card 00-047 and 01-085). The peak of FeSi is observed at $2\theta = 50.59°$ (2 1 1) (JCPDS card 01-086), and at $2\theta = 59.04°$, it corresponds to CaSi (2 1 5) plane diffraction (JCPDS card 01-076). The peak at $2\theta = 66.76°$ is credited to Al_2O_3 (2 1 1) (JCPDS card 00-002), while the peak at $2\theta = 74.09°$ corresponds to Fe_3O_4 (5 3 3) plane diffraction (JCPDS card 01-088).

The predominant crystal structure for TiO_2 is rutile, with peaks located at $2\theta = 27.72°$, $36.38°$, $41.48°$, $44.27°$, $54.56°$, $56.88°$, $64.31°$, $69.24°$, and $70.02°$, which correspond to the (1 1 0), (1 0 1), (1 1 1), (2 1 0), (2 1 1), (2 2 0), (3 1 0), (1 1 2), and (1 1 2) diffraction planes, respectively (JCPDS card 01-088). Additionally, the TiO_2 anatase phase exhibits peaks at $2\theta = 25.56°$ and $48.27°$, which correspond to the (1 0 1) and (2 0 0) diffraction planes, respectively (JCPDS card 01-083).

The diffraction peaks of TiO_2EFBA are distinctly different from EFBA, primarily due to the effective deposition of TiO_2 on the surface of EFBA, which are phase changes and rearrangement of the crystal phase. The growth of new metal oxide on TiO_2EFBA which are Al_2FeO_4, Fe_3O_4, $Mg_2Si_2O_6$, $CaSiO_3$, Fe_7S_8, $Fe_{0.5}Mg_{0.5}O_5Ti_2$, FeTiO5, $FeSiO_4$, FeS, Fe_3S_4, Al, Al_2O_3, FeO, KO_2, K_3P_{11}, and Fe_2O_5P confirm the chemical restructuring within EFBA. Moreover, the TiO_2EFBA was overlapped with the TiO_2 phase. According to Alterary & Marei., these metal oxides are considered stable phases in the reaction process [36]. Based on the FFA conversion, the metal oxide in the EFBA is expected to enhance the catalytic activity. As Reported by Li et al., the metal oxide can act as a co-catalyst in the reaction process, promoting the separation of charge carriers and the migration of the e^-/h^+ pair to the surface of TiO_2, which can enhance the photocatalytic efficiency

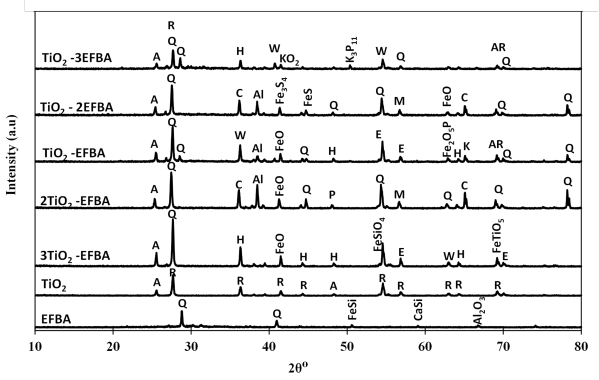

Figure 1. XRD patterns of EFBA, TiO_2, and with five different mass ratios of EFBA and TiO_2. The corresponding crystalline phase labelled as: A- Anatase (TiO_2); R- Rutile (TiO_2); C- Cristobalite (SiO_2); E- Enstatite ($Mg_2Si_2O_6$); H- Hercynite (Al_2FeO_4); K- Kennedyite ($Fe_{0.6}Mg_{0.6}O_5Ti_{1.8}$); M- Magnetite ($Fe_3O_4$); P- Pyrrhotite ($Fe_7S_8$); Q- Quartz ($SiO_2$); W- Wollastonite ($CaSiO_3$); AR- Armalcolite ($Fe_{0.5}Mg_{0.5}O_5Ti_2$); CaSi; FeSi; Iron Oxide (FeO); Iron Titanium Oxide ($FeTiO_5$); Iron Silicate ($FeSiO_4$); Iron Phosphate Oxide (Fe_2O5P); Smythite (Fe_3S_4); Iron Sulfide (FeS); Potassium Oxide (KO_2); Potassium Phosphide (K_3P11); Aluminum (Al); Aluminum Oxide (Al_2O_3).

and successfully produce the desired product [37].

The crystallinity of TiO_2EFBA after the doping technique is slightly increased compared to EFBA and TiO_2 as shown in Table 2 which was calculated using the Debye-Scherrer formula (equation 9). This result indicates that the doping technique supports TiO_2 recrystallization on EFBA, leading to increasing the catalytic performance during the reaction process. Based on the catalytic activity, TiO_2EFBA outperform TiO_2, with TiO_2EFBA converting 78% FAME compared to TiO_2 only 28%. Hence, increased crystallinity contributed to the enhanced photocatalytic performance of TiO_2EFBA. However, varying mass ratios of TiO_2EFBA significantly affect the photocatalytic performance, consistent with the finding by Song et al. Their study indicates that excessive concentrations of supporting materials and TiO_2 may introduces recombination centers and decrease the reaction rate also yield of the product [38].

$$D = k\lambda/\beta\cos\theta \tag{10}$$

Table 2. Crystallite size of EFBA, TiO_2, and TiO_2EFBA with five different ratios.

Catalyst	D(nm)
EFBA	43.84
TiO_2	37.65
$3TiO_2$EFBA	53.96
$2TiO_2$EFBA	55.75
TiO_2EFBA	50.89
$TiO_2$2EFBA	53.03
$TiO_2$3EFBA	50.20

where D represents the crystallite size, k is Scherrer constant (0.9), λ is the X-ray wavelength, β is the FWHM (full width at half maximum), θ is the difference angle.

3.2 SEM-EDX analysis

The morphology of the as prepared photocatalyst was observed using SEM analysis. Fig. 2 (a-c) displays the SEM images of EFBA, TiO_2, and TiO_2EFBA all magnified at 3000X. In Fig. 2 (a), EFBA appears to have a spherical shape with a rough surface and small pores that can improve their adsorption properties. This observation aligns with findings from previous studies [39–41]. Fig. 2 (c) showed the surface morphology of TiO_2 doped with EFBA. Here in Fig. 2 (b), TiO_2 is seen as relatively smooth and aggregated spherical particles. The images of TiO_2EFBA suggested that TiO_2 particles are effectively loaded onto the EFBA surface, with uniformly dispersed, and evenly distributed indicating the successful application of the impregnation method for TiO_2EFBA. Additionally, the unchanged spherical shape of TiO_2, as depicted in Fig. 2 (c), post-impregnation, suggests that TiO_2 remains a stable semiconductor photocatalyst, with no apparent physical damage incurred during the process. Li et al. stated that, metal oxide plays a vital role as it can contributed to the stability and durability of the photocatalyst, which protect the TiO_2 from degradation, leading to a longer lifespan for the reusability process [37].

EDX analysis was conducted to determine the elemental composition of the materials shown in the Fig. 2 (d). A particular region on the catalyst surface was designated for examination. The EDX outcomes for EFBA, TiO_2, and TiO_2EFBA at five distinct ratios are displayed in Table 3. The findings indicated the detection of Ti along with a new metal oxide element on the TiO_2EFBA catalyst. This implies that the formation of new metal oxides and recrystallization took place throughout the impregnation process. These observations are consistent with the XRD analysis, which also identified the presence of new metal oxides on TiO_2EFBA.

Fig. 2. (e) presents the mapping analysis of TiO_2EFBA at a 1:1 mass ratio. The presence of the Ti element verifies the incorporation of TiO_2, which appears as clusters attached to the EFBA matrix. Furthermore, Fig. 2 (e) illustrates the various elements within the TiO_2EFBA structure, distinguished by distinct colors, representing varying concentrations of elements including, Ti, O, Si, C, K, and Ca.

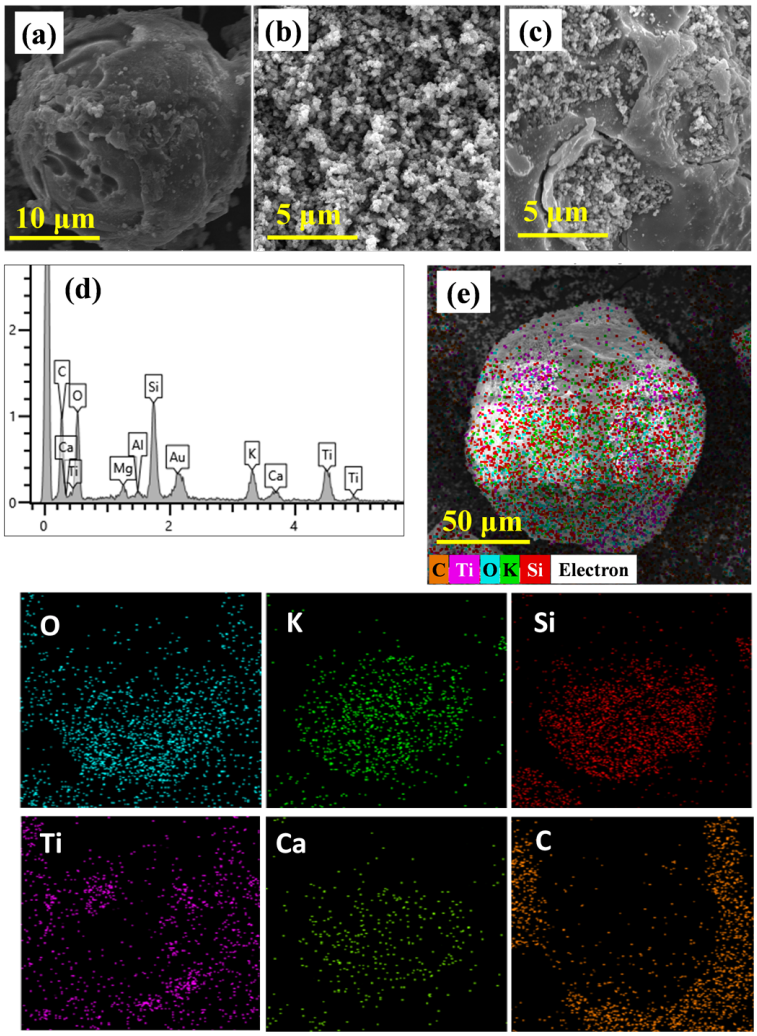

Figure 2. SEM image of the a) EFBA b) TiO_2 and c) TiO_2EFBA, d) EDX spectrum, and e) Mapping of the chemical elements of TiO_2EFBA 1:1 mass ratio.

Table 3. Elemental composition of EFBA, TiO_2 and TiO_2: EFBA with various mass ratio characterized by EDX analysis.

Catalyst	Elemental composition (wt.%)											
	Ti	O	C	Si	K	Mg	Ca	Al	P	Fe	Cl	F
EFBA	-	60.02	19.49	3.48	11.19	0.53	1.65	-	-	-	3.08	-
TiO_2	52.41	47.59	-	-	-	-	-	-	-	-	-	-
3TiO_2-EFBA	45.28	41.01	5.48	1.63	1.00	0.22	0.60	1.01				3.78
2TiO_2-EFBA	31.40	39.71	20.22	2.48	-	0.26	0.81	1.28	-	-	-	2.59
TiO_2-EFBA	26.52	39.81	23.80	3.79	3.37	0.48	1.05	0.84			0.34	
TiO_2-2EFBA	39.40	40.72	3.49	6.04	4.66	0.65	2.32	1.29	0.46	0.98	-	-
TiO_2-3EFBA	26.25	43.43	12.56	4.10	8.29	0.35	1.67	0.93	0.49	-	1.93	-

This observation confirms the existence of quartz, wollastonite, and other metal oxides in the TiO_2-doped EFBA, also in different mass ratios of the catalyst. According to Mares et al., metal oxide compounds play a vital role in biodiesel production, as the properties of alkaline metals contribute to the high catalytic activity during the reaction process. SEM-EDX analysis on TiO_2EFBA confirmed the successful application of TiO_2 on the EFBA's matrix with homogeneous distribution [42].

3.3 FTIR analysis

The characterization of functional groups within the materials was conducted using FTIR spectroscopy, as depicted in Fig. 3 . In the spectral region ranging from 470 to 490 cm^{-1}, a distinctive band emerged, which corresponds to the O-Ti-O bridging vibration characteristic of rutile TiO_2. In the same spectral range for EFBA, the presence of a metal oxide compound was evident, indicative of oxygen bonds with iron and silica, denoted as O-Si and O-Fe. At the wavenumber of 496.03 cm^{-1}, a notable shift in bonding from Fe-O to Fe-Ti was observed [43]. Furthermore, a band at 796.44 cm^{-1} was attributed to the functional group of TiO_2, originating from both Ti-O and Ti-O-Ti bonds. The peak at 844.87 cm^{-1} pointed to the incorporation of Ti onto the EFBA surface, signifying the establishment of Ti-O-metal oxide bonds in TiO_2EFBA. The presence of a broad peak at 3687.27 cm^{-1} was indicative of OH bonds in water molecules adsorbed by TiO_2 [44]. Additionally, a sharp band at 1256.91 cm^{-1} was assigned to the Ti-O-C bond. A noteworthy distinction among EFBA, TiO_2, and TiO_2EFBA

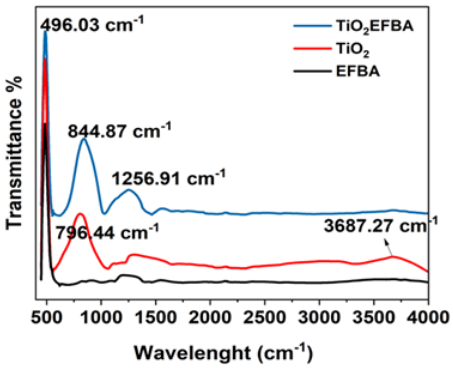

Figure 3. FTIR spectra of EFBA, TiO_2 and TiO_2-EFBA.

was the alteration in wavenumbers. Specifically, following the impregnation process, the wavenumber shifted from 796 to 844 cm^{-1} and from 470 to 496 cm^{-1}. This aligns with the XRD results, which substantiated that TiO_2 had effectively become integrated within the EFBA matrix, as depicted by the observed spectral changes.

3.4 UV-Vis DRS analysis

A UV-visible diffuse reflection spectroscopy (UV-Vis DRS) was conducted to determine the band gap energy of a photocatalyst. The investigation focused on TiO_2 and TiO_2EFBA with varying mass ratios. The band gap energy values were calculated using the Tauc plot equation (hv versus $(\alpha hv)^{1/2}$) using (equation 11), and the graph was illustrated in Fig. 4. The results revealed that the band gap energy decreased after the wet impregnation process, specifically when using a 1:1 weight ratio of TiO_2-EFBA, resulting in a value of 2.92 eV. This decrease in band gap energy led to increased light absorption in the 400-500 nm range, a lower energy region in which the catalyst can maintain high photocatalytic activity at a high range of wavelengths. Moreover, EFBA can serve as a trapping agent, effectively capturing electron and hole pairs and reducing the probability of recombination, thereby helps in enhancing the photocatalytic esterification process [45].

Observations indicated that excessive doping ratios of TiO_2 and EFBA slightly increased the band gap energy, thereby inhibiting photocatalytic esterification. The band gap energy values for TiO_2EFBA ratios of 3:1, 2:1, 1:2, and 1:3 were 3.01 eV, 3.02 eV, 3.04 eV, and 3.02 eV, respectively, slightly higher than that of pure TiO_2 (3.0 eV). This indicated that, there is no significant in increasing and decreasing the mass ratio of TiO_2 and EFBA. Existing literature suggested that the appropriate amount of doping-supporting materials with TiO_2 introduces a new energy level below the conduction band of TiO_2 [38]. Therefore, the 1:1 mass ratio of TiO_2 and EFBA is an appropriate ratio to enhance the performance of the photocatalytic activity.

The band gap energy can be calculated using the following equation:

$$\alpha hv = A(hv - E_g)^{n/2} \tag{11}$$

where α is the absorption coefficient, hv is the photon energy, A is a constant, and E_g is the bandgap energy in which $n = 1$ for direct bandgap material. The direct bandgap energy in Fig. 4 is determined by extrapolation of the linear part of the graphics to the axis of the abscissa.

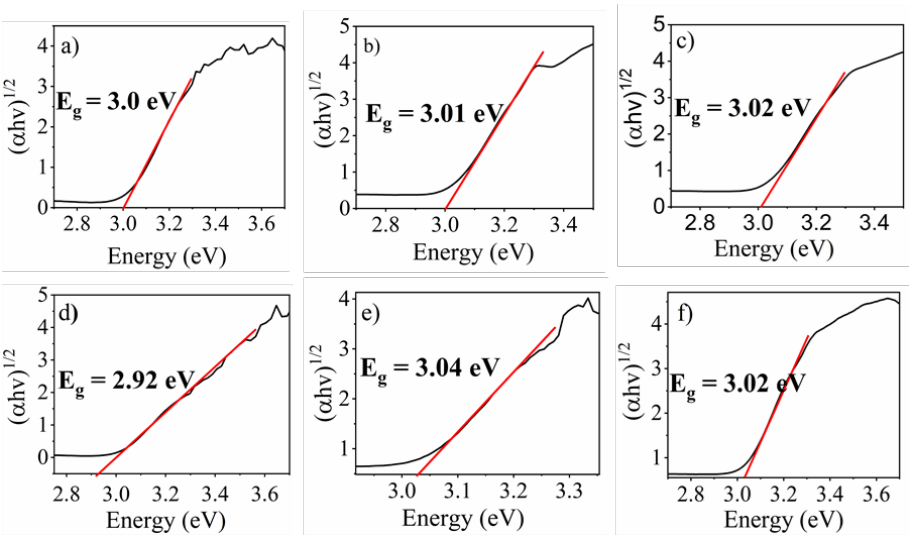

Figure 4. . Band gap energy (E_g) spectrum of a) TiO_2, b) 3TiO_2-EFBA, c) 2TiO_2-EFBA, d) TiO_2-EFBA, e) TiO_2-2EFBA and f) TiO_2-3EFBA.

3.5 XRF analysis

The presence of inorganic elements in both fresh and spent TiO_2EFBA catalysts was assessed using X-ray fluorescent (XRF) analysis, with the results presented in Table 4. There was a minimal decrease observed in the concentrations of TiO_2 and other metal oxides between the fresh and spent catalysts. Fresh TiO_2 constitutes about 70.5 wt%, and at the 10th cycle, the compositions decrease to only 64.1 wt%. For the metal oxides in the EFBA, also slightly decrease. Consequently, the reduction in the FFA conversion percentages when using both fresh and spent catalysts was only slight. This can be attributed to the TiO_2EFBA catalyst's ability to maintain the active sites on its surface and uphold its photocatalytic performance.

3.6 Catalytic activity

The optimal conditions for photo-esterification were initially evaluated on TiO_2 and 1:1 ratio of TiO_2EFBA under 365 nm UV light. Subsequent tests involved varying the ratios and utilizing different light sources, including visible and xenon light. The outcomes revealed that both TiO_2 and TiO_2EFBA performed best under the same conditions: 2 h reaction time, 20:1 methanol to WCO molar ratio, and 4 wt.% catalyst loading. Notably, the FFA conversion using TiO_2EFBA reached 78%, while TiO_2 alone achieved only 28%. These results highlight the superior supportive role of EFBA in enhancing the FFA conversion rate when combined with TiO_2. This enhancement can be attributed to EFBA's ability to modify the semiconductor properties of TiO_2 and regulate its band gap energy, as confirmed by the catalyst's characterization.

Table 4. The component analyzed in oxide by weight percent (wt%) calculated using XRF analysis for fresh and spent TiO_2-EFBA.

Component (wt%)	Fresh catalyst	1^{st} cycle	10^{th} cycle
TiO_2	70.5	73.9	64.1
SiO_2	10.1	10.6	17.4
K_2O	9.61	6.06	5.05
CaO	2.77	2.93	3.62
Al_2O_3	2.68	2.35	2.61
Fe_2O_3	1.26	1.2	1.16
Cl	1.15	0.18	0.03
P_2O_5	0.977	0.983	1.52
MgO	0.371	0.784	1.67

The optimization parameters for the esterification reaction were investigated using the Langmuir-Hinshelwood-Hougen-Watson (LHHW) kinetic model. This model involves adsorption, surface reaction, and desorption of atoms and molecules on the surface [46, 47]. FFAs and methanol are initially adsorbed onto the photocatalyst surface, and the reaction took places when the e^-/h^+ transform these molecules into free radicals. These free radicals then undergo intermediate processes leading to the formation of the product FAME and water molecules. Finally, the adsorbed products are desorbed. A Detailed elucidation of this mechanism is provided in the mechanism section.

As depicted in Fig. 5 (a), when employing a 20:1 methanol to WCO molar ratio with 4 wt.% of both TiO_2 and TiO_2EFBA catalysts, the conversion rates were 20% and 48% at 1 h reaction time, respectively. These rates increased to 28% and 78% when the reaction time was extended to 2 h. Thus, a slightly longer reaction duration can elevate the conversion percentage, primarily because a 2 h span minimizes mass transfer limitations, achieved an equilibrium state of the reaction. However, prolong the reaction time can be detrimental, as noted by the decline in FFA conversion rates. According to Lam & Lee., once methanol reaches equilibrium, the photo-esterification process tends to revert due to its reversible nature [48]. The reversible nature of esterification hinders production once the reaction attains an equilibrium point where the forward reaction rate is equal to the reverse reaction rate. As a result, the reaction never proceeds to completion but rather reaches an equilibrium state. This phenomenon was similarly noted by Onukwuli

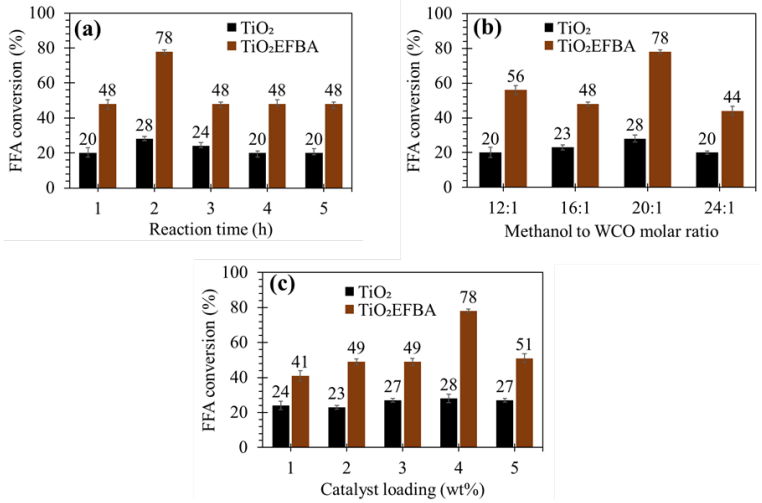

Figure 5. Effect of operating parameter on FFA conversion (%) of WCO: a) reaction time (TiO_2 and TiO_2EFBA_ 20:1 methanol to WCO molar ratio and 4 wt% catalyst) b) methanol to WCO molar ratio (TiO_2 and TiO_2EFBA_ 2 h reaction time and 4 wt% catalyst) c) catalyst loading TiO_2 and TiO_2EFBA_ 20:1 methanol to WCO molar ratio and 2 h reaction time.

et al., who observed that the slow adsorption of reactants onto the catalyst surface impedes the reaction from interacting with photoinduced e^-/h^+, thereby diminishing the conversion percentage. For TiO_2, the conversion decreased to 24% at 3 h and remained consistent at 20% for 4 and 5 h. Conversely, TiO_2EFBA exhibited a reduction to 48% at 3 h, stabilizing thereafter. Based on these findings, a 2 h reaction time appears to be optimal, achieving a 78% FFA conversion rate under UV light conditions.

The FAME was produced by the presence of alcohol, as depicted in Fig. 6. Methanol was selected for this study due to its favorable physical and chemical properties. Theoretically, the stoichiometry of methanol to oil molar ratio for the reaction process is 3:1 [49]. However, excess methanol is required to push the equilibrium towards the FAME formation [50]. In this research, the methanol to WCO molar ratios tested ranged from 12:1 to 24:1 while maintaining a 4 wt.% catalyst concentration and a 2 h reaction time. As illustrated in Fig. 5 (b), an increase in methanol quantity corresponds to a higher FFA conversion. For TiO_2 catalyst, the conversion rates were 20% at a 12:1 molar ratio, 23% at 16:1, and peaked at 28% at 20:1. However, further increasing the methanol amount led to a decline in the conversion rate, dropping back to 20% at a 24:1 molar ratio. A similar trend was observed with the TiO_2EFBA catalyst. At a 12:1 molar ratio, the conversion rate stood at 56%, only slightly dropping to 48% at 16:1. As highlighted by Ghani et al., insufficient methanol quantities below a specific threshold can impede the photo-esterification reaction. However, when the methanol ratio was increased to 20:1, the conversion rate surged to 78% [51]. Yet, further elevating the ratio to 24:1 led to a decline in the conversion rate to 44%. Consistent with findings by Gohain et al., an excess of methanol can limit the attachment of more FFA to the catalyst's surface, thus slowing down the reaction [52]. The results suggest that TiO_2EFBA outperforms TiO_2, which is further supported by the bandgap energy data, indicating that TiO_2EFBA has a narrower bandgap, allowing it to function effectively under 365 nm UV light irradiation. Additionally, EFBA's metal oxide components enhance the catalytic activity, facilitating charge carrier separation and reducing the recombination rate of e^-/h^+ pairs, thereby promoting the conversion of FFA to the desired FAME product. In this reaction, a semiconductor photocatalyst was utilized, as UV light is essential for activating TiO_2EFBA and initiating the formation of e^-/h^+ pairs. These e^-/h^+ pairs subsequently interact with methanol and FFA to generate the FAME. Fig. 5 (c) illustrates the impact of catalyst concentration on FFA conversion. The results indicate that FFA conversion improves with increasing catalyst concentration. Specifically, with TiO_2, the conversion rates were 24% at 1 wt%, 23% at 2 wt%, a slight increase to 27% at 3 wt%, and a peak of 28% at 4 wt%. However, at 5 wt%, the conversion rate reduced marginally to 27%. Conversely, for TiO2EFBA, the conversion rate was 41% at 1 wt%, rising to 48% at both 2 wt% and 3 wt%. A significant jump

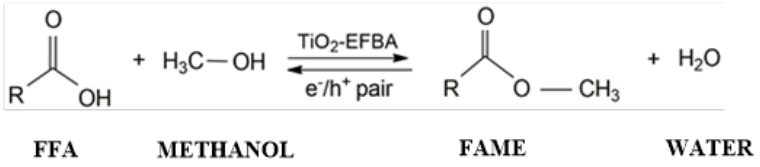

Figure 6. Reaction pathway of photo-esterification reaction.

was observed at 4 wt%, reaching 78%, before declining to 57% at 5 wt%. The findings suggest that an increase in catalyst concentration enhances FFA conversion due to the increased active sites available in the reaction. This intensify surface area exposure to e^-/h^+ pairs facilitate interactions with methanol and FFA, promoting the reaction. However, a decline in conversion was observed beyond a 4 wt% catalyst loading. As noted by Lam & Lee, once a minimal quantity of FAME is generated, biodiesel can serve as a co-solvent, enhancing system solubility without relying on methanol [48]. It becomes evident that only a specific catalyst amount is optimal for the reaction, with further increases resulting in negligible conversion improvements. Additionally, Redjeki et al. highlighted that an excessive catalyst concentration can induce turbidity during the reaction, limiting light penetration and subsequently reducing photocatalytic efficiency [53].

3.7 Photocatalytic activity using different mass ratio of TiO_2 and EFBA

In this research, various mass ratios of TiO_2EFBA were examined, denoted as (x-TiO_2: y-EFBA); specifically, (3x:1y, 2x:1y, 1x:1y, 1x:2y, and 1x:3y). As illustrated in Fig. 7, the 1:1 ratio of TiO_2EFBA yielded the highest conversion rate at 78%, outperforming the other ratios 3TiO_2EFBA, 2TiO_2EFBA, $TiO_2$2EFBA and $TiO_2$3EFBA which achieved 42%, 27%, 42%, and 46%, respectively. This highlights the significance of band gap energy in the photo-esterification process, as the 1:1 ratio of TiO_2EFBA displayed the narrowest band gap energy among the tested ratios. A reduced band gap energy enhances photocatalytic activity and enhances light absorption by TiO_2EFBA, thereby sustaining the photo-esterification reaction. Consequently, altering the mass ratio of either TiO_2 or EFBA can elevate the band gap energy, diminishing light absorption in the semiconductor catalyst. In line with research by Gnanaprakasam et al., an increased mass ratio of TiO_2 or EFBA compromises the photocatalyst's stability, consequently lowering the conversion rate [54]. This is attributed to the excessive doping of TiO_2 with a minimal amount of support material, which hampers the catalyst's efficiency. The optimal mass ratio of TiO_2EFBA is determined to be 1:1, as it strikes the perfect balance, yielding the desired product and ensuring superior photocatalytic performance.

3.8 Photocatalytic activity on TiO_2EFBA using different intensity of light sources

The experiment was further prolonged to assess the reaction under various light conditions: without any light source, under UV light at 254 nm (6 watt), visible light (23 watt), and a xenon lamp (250 watt). These evaluations were conducted using the optimized parameters of a 4 wt% TiO_2EFBA catalyst, a 20:1 methanol to WCO molar ratio, and a 2 h reaction time. As depicted in Fig. 8, the reaction conducted without any light source resulted in a mere 10% conversion of FFA. This emphasizes that TiO_2EFBA remains inactive in the absence of light, failing to produce the necessary e^-/h^+ pairs vital for interacting with methanol and FFA, thereby hindering the conversion to FAME.

Under exposure to UV light with a 254 nm wavelength (short-wave), the conversion rate of FFA rose to 46%. However, when utilizing a UV light with a longer wavelength of 365 nm (long-wave), this rate surged to 78%. This pattern indicates that TiO_2EFBA catalyst, with a bandgap energy of 2.92 eV, resonates more effectively with the energy spectrum of the 365 nm UV light compared to the 254 nm wavelength. As a result, TiO_2EFBA demonstrates superior photon absorption and a raise generation of e^-/h^+ pairs when illuminated with the 365 nm UV light. In contrast, the 254 nm UV light delivers an energy level that is not efficiently utilized in the photocatalytic reaction.

Furthermore, TiO_2EFBA displays limited responsiveness when exposed to visible and xenon light, yielding conversion rates of only 46% and 54% for FFA, respectively. This behavior can be attributed to the bandgap energy of TiO_2EFBA, which stands at 2.92 eV, aligning more closely with the absorption edge suitable for UV light irradiation. The findings suggest that when TiO_2EFBA is illuminated by visible light or xenon light, the catalyst struggles to effectively absorb photons and generate e^-/h^+ pairs. This is because visible light and xenon lights possess lower photon energies and longer wavelengths than the 365 nm UV light. Consequently, these light sources fail to supply the requisite energy to surpass the bandgap energy of TiO_2EFBA. To enhance its efficacy under visible or xenon light, TiO_2EFBA would require modifications in its band structure and photo-

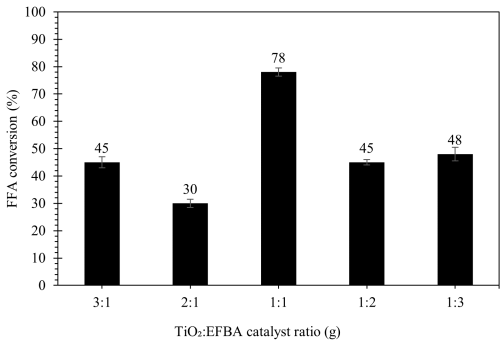

Figure 7. FFA conversion of esterified WCO with different mass ratio of TiO_2 and EFBA (2 h reaction time, 20:1 methanol/WCO molar ratio and 4 wt% catalyst).

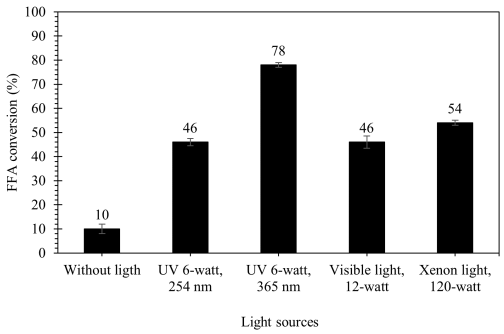

Figure 8. FFA conversion of esterified WCO with different type of light sources; with reaction condition (2 h reaction time, 20:1 methanol/WCO molar ratio and 4 wt% catalyst).

catalytic properties to accommodate lower photon energies that are less potent than UV light.

3.9 Reusability test

A reusability test was conducted on the TiO_2EFBA catalyst with a 1:1 mass ratio. The catalyst was retrieved through filtration and subsequently rinsed with hexane to eliminate any residual of esterified WCO stick to its surface. The recovered catalyst was then subjected to multiple reuse cycles under the specified conditions: 4 wt% TiO_2EFBA catalyst concentrations, 20:1 methanol to WCO molar ratio, and 2 h reaction time. Fig. 9 illustrates the result of the reusability test. The data revealed that TiO_2EFBA catalyst retains its functionality over 10 cycles of photo-esterification, with only a slight decline in FFA conversion when compared to using fresh catalyst. Specifically, the FFA conversion rates were 78% in the initial cycle, 75% in the second and third cycles, 72% in the fourth cycle, and a gradual decrease to 67% by the fifth cycle, persisting steadily through the tenth cycle.

Throughout the reusability trials, the TiO_2EFBA catalyst consistently maintained an impressive conversion rate exceeding 50%. They attributed this decline to the obstruction of active sites by residual esterified WCO stick to the catalyst's surface [51]. Additionally, the washing process with hexane during the catalyst's retrieval could have contributed to a decrease in active sites, thereby impacting the overall catalytic efficiency. Moreover, this result was aligned with XRF analysis when using a fresh catalyst; the conversion FFA up to 78% and a slight decline in TiO_2 component at the 10^{th} cycle reduced the yield of conversion. However, despite these minor setbacks, TiO_2EFBA demonstrated a high stability in its photocatalytic performance over the ten reuse cycles. The EFBA component emerged as an invaluable support material, safeguarding the photocatalyst from deterioration under harsh conditions and optimizing the recycling potential of TiO_2EFBA.

3.10 Scavenger test

The identification of reactive species participating in the photocatalytic process was accomplished through experiments utilizing Active Species Trapping (AST). In this investigation, scavenger agents such as ethylenediaminetetraacetic acid (EDTA), p-Benzoquinone (p-BQ), isopropanol (IPA) and silver nitrate ($AgNO_3$) were employed to capture photogenerated h^+, $(CH_3CO\bullet)OH$ radical, $CH_3O\bullet$ radical and photogenerated e^-, respectively. These scavenger agents were utilized to trap the active species during the reaction, thereby suppressing photocatalytic activity. As illustrated in Fig. 10, the addition of scavenger agents to the photocatalytic system led to a decrease in photocatalytic activity compared to situations where no scavenger agent was added. The introduction of EDTA, p-BQ, IPA and $AgNO_3$ resulted in a reduction of FFA conversion from 78% to 40.64%, 40.72%, 30.81%, and 32.5%, respectively. This outcome suggests that photogenerated h^+, $(CH_3CO\bullet)OH$ radicals, $CH_3O\bullet$ radicals and photogenerated e^- serve as active species in the photo-esterification mechanism.

As reported by Coleto et al., there are subtle differences among these three active species in terms of direct and indirect reactions [55]. They propose that holes directly oxidize species adsorbed on the surface of particles, whereas electrons first reduce the adsorbed oxygen, which then reacts with species. Therefore, the introduction of scavenger agents deactivated the active species of TiO_2EFBA, consequently reducing the conversion of FFA. The experiment highlights the successful conversion of FFA attributed to the active species of electronic charge in the photocatalytic system, suggesting potential applications for further research.

3.11 Pathway mechanism of TiO_2-EFBA in photocatalytic esterification

The metal oxides within EFBA serve as trapping agents, aiding in the separation of e^-/h^+ pairs during oxidation and reduction. SiO_2 and K_2O are key metal oxides identified in EFBA, crucial for this process. They trap e^-, slowing down their recombination rate, which improves catalyst performance. Introducing new energy levels within TiO_2 reduces bandgap energy, allowing the catalyst to absorb more photons and generate additional e^-/h^+ pairs, enhancing FFA conversion. XRD and SEM-EDX analyses confirm the uniform distribution of TiO_2 onto the EFBA lattice.

The scavenger test explored the mechanism within the photocatalytic system (Fig. 10), utilizing the Langmuir Hinshelwood reaction pathway for biodiesel production. When UV light activates TiO_2EFBA, it generates e^-/h^+ pairs,

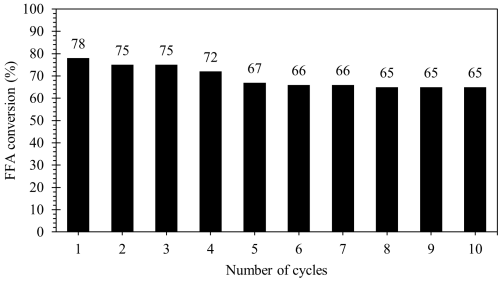

Figure 9. Reusability test of TiO_2EFBA on photo-esterification WCO using optimized parameter of 2 h reaction time, 20:1 methanol/WCO molar ratio and 4 wt% catalyst.

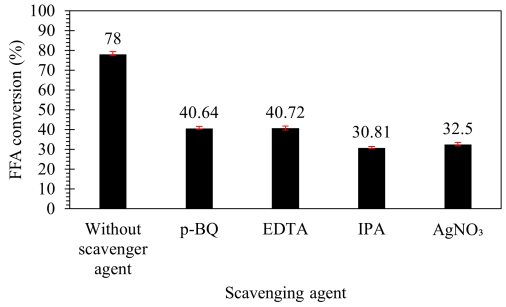

Figure 10. Effect of different scavenger on photo-esterification on TiO_2EFBA. Condition: 2 h reaction time, 20:1 methanol to WCO molar ratio and 4 wt% catalyst loading.

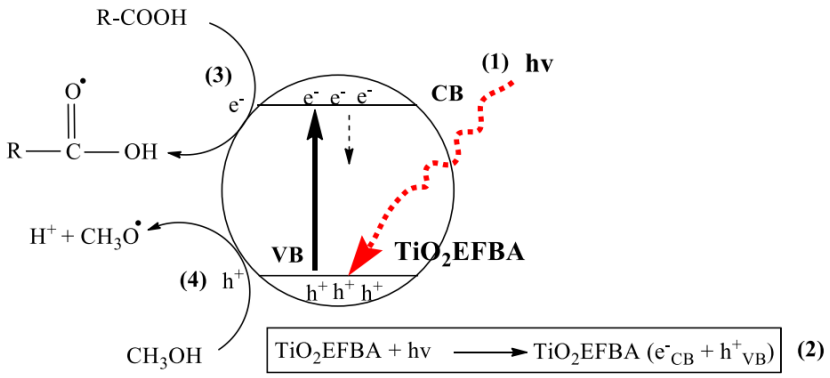

Figure 11. Mechanism of photocatalytic reaction on esterification of waste cooking oil catalyzed by TiO_2EFBA under UV light irradiation (365 nm).

which migrate to the surface and catalyze chemical reactions. Methanol (CH_3OH) adsorbs onto lattice oxygen atoms, acting as Lewis basic sites, while FFAs (RCOOH) adheres to Ti^{4+} ions, serving as Lewis acid sites in the photo-esterification process proposed by Corro et al. [56]. Based on the experimental findings above, the mechanism has been elucidated as depicted in Fig. 11. In the initial step (1), when the TiO_2EFBA catalyst is illuminated by photons, it generates e^-/h^+ pairs (step 2). The e^- transitions from the VB to the CB, leaving behind h^+. During the esterification process, CH_3OH and R-COOH diffuse to the surface of TiO_2EFBA. Upon adsorption of R-COOH on the photocatalyst's surface, it undergoes reduction by e^- to form ROS species (RCO•) OH radicals (step 3). Simultaneously, CH_3OH adsorbed on the photocatalyst's surface reacts with h^+ to generate CH_3O• radicals and H^+ (step 4). The produced CH_3O• radicals attack the carbonyl group of (RCO)•OH radicals to form a tetrahedral intermediate compound (step 5). Subsequently, the tetrahedral intermediate undergoes decomposition via proton transfer and loss of a leaving group. Proton transfer occurs as the oxygen atom within the tetrahedral intermediate, carrying a negative charge, abstracts a proton from a CH_3OH molecule, leading to the generation of hydroxide ions and regeneration of the carbonyl oxygen (step 6). The hydroxide ions act as a base and abstract a proton from the CH_3OH molecule attached to the carbonyl carbon, resulting in the elimination of a water molecule (step 7). The resulting product is desorbed from TiO_2EFBA surface and separated into the liquid phase (step 8) [53] (Appendix).

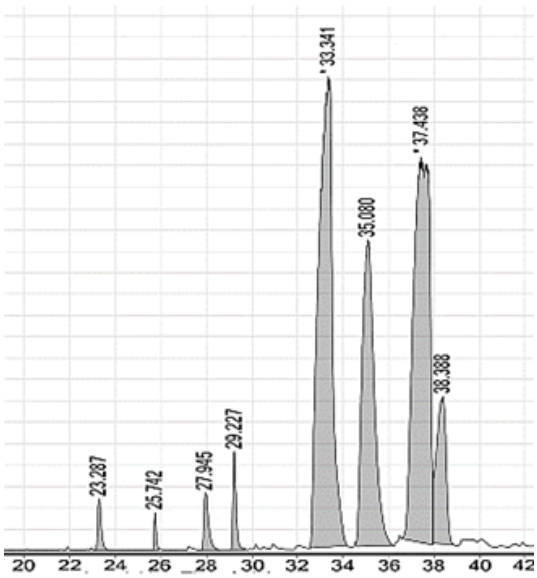

Figure 12. GCMS analysis of FAME product

3.12 GCMS analysis of FAME

The composition of biodiesel was analyzed using gas chromatography mass spectroscopy (GCMS). As depicted in Fig. 12, and Table 5 the predominant component was hexadecanoic acid, also known as C16 methyl ester, constituting 35% of the total composition. This was followed by octadecanoic acid (C18) at 33%, octadecadienoic acid (C18:2) at 8%, tetradecanoic acid (C14) at 3.1%, and dodecanoic acid (C13) at 1.4%. Based on the yield calculation, the conversion rate of FAME was determined to be 78%. These results highlight the significant production of FAME,

Table 5. Composition of FAME in WCO biodiesel.

Retention time (min)	Fatty acid compound (methyl ester)	Composition (%)
22.287	Dodecanoic acid	1
25.742	Dodecanoic acid	0.4
27.945	Tetradecanoic	1.4
29.227	Tetradecanoic	1.7
33.341	Hexadecanoic acid	35
35.080	Heptadecanoic acid	20
37.438	Octadecenoic acid	33
38.388	Octadecadienoic acid	8

which can be attributed to the substantial reduction in the FFA content of the WCO from 12.4 wt% to 2.7 wt%. This decrease in FFA content is crucial as it helps prevent saponification, thereby ensuring a higher yield of biodiesel.

4. Conclusions

WCO exhibits a high content of FFA at 12.4 wt% with an acid value of 24.8 mg KOH g^{-1}. This study investigates into a two-step reaction approach. Initially, a photocatalyst TiO_2EFBA is employed under light exposures to reduce the FFA content in the feedstock oil and convert it into FAME. Then, a conventional method utilizing NaOH catalyst is utilized to convert triglycerides into FAME. The photocatalyst is synthesized through a wet impregnation technique with continuous stirring at room temperature for 1 h. During the first step, FFA conversion to FAME reaches 78%, reducing FFA from 12.4 wt% to 2.72 wt%. This is achieved by utilizing a 1:1 mass ratio of TiO_2EFBA, exposed to UV light of 6-watt 365 nm irradiation, under optimized conditions: 2 h reaction time, 20:1 methanol to WCO molar ratio, and 4 wt% catalyst loading at room temperature. XRD analysis confirms the integration of TiO_2 onto the surface of EFBA and enhanced the crystallite size of TiO_2EFBA compare to TiO_2 and EFBA. UV Vis DRS analysis indicates a reduction in bandgap energy from 3.0 eV of TiO_2 to 2.92 eV of TiO_2EFBA, attributed to the presence of metal oxides narrowing down the bandgap energy of TiO_2. XRF analysis reveals minimal leaching of active components from the catalyst, signifying its high stability and potential for reuse up to 10 cycles without compromising photocatalytic performance. Scavenger reaction revealed photogenerated h^+ and e^- assisted (RCO•) OH radicals and CH_3O• radicals in converting to FAME. Thus, the TiO_2EFBA catalyst plays a crucial role in mitigating high FFA levels in WCO, exhibit its resilience and potential as a photocatalyst for addressing the high FFA content of low-quality feedstock oils, thereby enhancing biodiesel production processes.

Acknowledgment
The Authors acknowledge the Ministry of Higher Education (MOHE) for funding under the Fundamental Research Grant Scheme (FRGS) (FRGS/1/2021/STG05/UITM/02/4).

Appendix

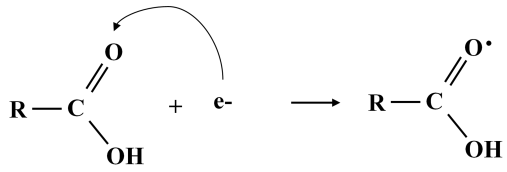

3 and 4: The electron at the surface of TiO_2EFBA attack on FFAs molecules forming FFAs radical $(CH_3CO•)OH$. The CH_3OH involved in the oxidation process where CH_3OH oxidized by a positive hole to form a CH_3O• radical H^+.

$$CH_3O\cdots H + (h^+) \longrightarrow CH_3O\cdot + H^+$$

5: The CH_3O• radical then attacks the $(CH_3CO•)OH$ radical, giving rise to intermediate compounds.

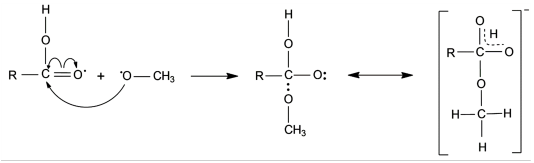

6: These intermediates undergo rearrangement process.

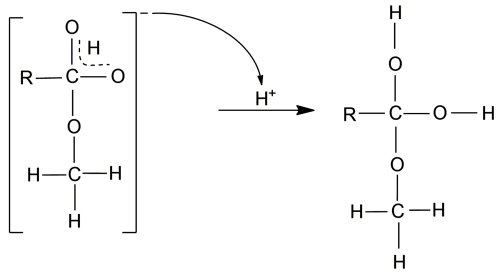

7: The process of dehydration to the formation of biodiesel.

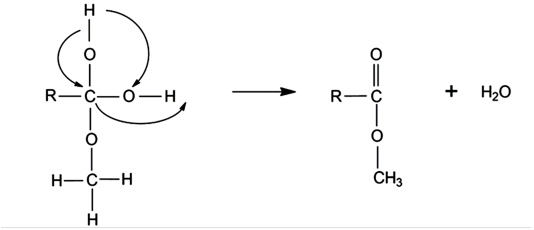

8: Last step, the resulting product is desorbed from the TiO_2EFBA surface and separated into the liquid phase. Vigorous stirring plays a crucial role in facilitating the adsorption of reactants and the desorption of products. This action accelerates the transfer rates of both reactants and products at the interface between phases.

Authors Contributions
Authors have equal contribution role in preparing the paper.

Availability of Data and Materials
The data that support the findings of this study are available from the corresponding author upon reasonable request.

Conflict of Interests
The authors declare that they have no known competing financial interests or personal relationships that could have appeared to influence the work reported in this paper.

References

[1] International Energy Agency, Oil Market Report. www.iea.org/reports/oil-market-report-november-2023. (2023):6 – 11, 2023.

[2] A. Galadima, O. Muraza, and J. Clean. . *Prod*, **263**(2020):121358. DOI: https://doi.org/10.1016/j.jclepro.2020.121358.

[3] S. Chozhavendhan, M. Vijay-Pradhap-Singh, B. Fransila, R. Praveen-Kumar, and G. Karthiga-Devi. . *Curr. Res. Green Sustain. Chem*, **1–2** (2020):1–6. DOI: https://doi.org/10.1016/j.crgsc.2020.04.002.

[4] A.S. Adekunle, J.A.O. Oyekunle, A.I. Oduwale, Y. Owootomo, O.R. Obisesan, S.E. Elugoke, S.S. Durodola, S.B. Akintunde, and O.S. Oluwafemi. . *Energy Reports*, **6**(2020):2861–2871. DOI: https://doi.org/10.1016/j.egyr.2020.10.019.

[5] A.S. Elgharbawy, W.A. Sadik, O.M. Sadek, M.A. Kasaby, and J. Chil. . *Chem. Soc*, **65**(2021): 5098–5109. DOI: https://doi.org/10.4067/S0717-97072021000105098.

[6] M. Hanif, I.A. Bhatti, M. Zahid, and M. Shahid. . *Sci. Rep*, **12**(2022)(1):1–14. DOI: https://doi.org/10.1038/s41598-022-20856-7.

[7] A. Naeem, I. Wali-Khan, M. Farooq, T. Mahmood, I. Ud-Din, Z. Ali-Ghazi, and T. Saeed. . *Bioresour. Technol*, **328**(2021):124831. DOI: https://doi.org/10.1016/j.biortech.2021.124831.

[8] K. Nisa, D.A.A. Salwa, A. Hasanah, and W. Widayat. . *AIP Conference Proceedings*, **2217**(2020). DOI: https://doi.org/10.1063/5.0000912.

[9] S.F. Wong, A.N.T. Tiong, and Y.H. Chin. . *Biofuels*, **14**(2023)(9):967–977. DOI: https://doi.org/10.1080/17597269.2023.2196804.

[10] O. Oloruntoba and A. Hamza. . *Food. Environ. Saf. J*, **18**(2019):89–96.

[11] P. Dhull, A. Sudhaik, V. Sharma, P. Raizada, V. Hasija, N. Gupta, T. Ahamad, V.H. Nguyen, A. Kim, M. Shokouhimehr, S.Y. Kim, Q.V. Lee, and P. Singh. . *Mol. Catal*, **539**(2023):113013, . DOI: https://doi.org/10.1016/j.mcat.2023.113013.

[12] A.A. Parwaz-Khan, P. Singh, P. Raizada, A. Khan, A.M. Asiri, and M.M. Alotaibi. . *Chemosphere*, **316**(2023):137839. DOI: https://doi.org/10.1016/j.chemosphere.2023.137839.

[13] A. Kumar, P. Singh, V.H. Nguyen, Q. Van-Le, T. Ahamad, S. Thakur, L. H. Nguyen, and P. Raizada. . *Chem. Eng*, **474**(2023):145720. DOI: https://doi.org/10.1016/j.cej.2023.145720.

[14] N. Skillen, H. Daly, L. Lan, M. Aljohani, C.W.J. Murnagham, X. Fan, C. Hardacre, G. N. Sheldrake, and P. K. J. Robertson. . *Top. Curr. Chem*, **380**(2022). DOI: https://doi.org/10.1007/s41061-022-00391-9.

[15] G. Corro, N. Sánchez, U. Pal, S. Cebada, and J.L.G. Fierro. . *Appl. Catal. B: Environ*, **203**(2017):43–52, . DOI: https://doi.org/10.1016/j.apcatb.2016.10.005.

[16] P. Dhull, A. Sudhaik, P. Raizada, S. Thakur, V. H. Nguyen, Q.V. Le, N. Kumar, A.A. Parwaz-Khan, H. M. Marwani, R. Selvasembian, and P. Singh. . *Chemosphere*, **333**(2023):138873, . DOI: https://doi.org/10.1016/j.chemosphere.2023.138873.

[17] A.A. Parwa-Khan, P. Singh, P. Raizada, A. Khan, A.M. Asiri, and M.M. Alotaibi. . *Chemosphere*, **316**(2023):137839. DOI: https://doi.org/10.1016/j.chemosphere.2023.137839.

[18] S.A. Younis, E.E. Kwon, M. Qasim, K.H. Kim, T. Kim, D. Kukkar, X. Dou, and I. Ali. *Prog. Energy Combust. Sci*, **81**(2020):100870. DOI: https://doi.org/10.1016/j.pecs.2020.100870.

[19] D. Masih, Y. Ma, and S. Rohani. *Appl. Catal B Environ*, **206**(2017):556–588. DOI: https://doi.org/10.1016/j.apcatb.2017.01.061.

[20] R. Ameta, M.S. Solanki, S. Benjamin, and S.C. Ameta. *Emerg. Green Chemical Technol*, (2018):135–175. DOI: https://doi.org/10.1016/B978-0-12-810499-6.00006-1.

[21] S. Varnagiris, A. Medvids, M. Lelis, D. Milcius, A. Antuzevics, and J. Photochem. *Photobiol. A Chem*, **382**(2019):111941. DOI: https://doi.org/10.1016/j.jphotochem.2019.111941.

[22] A. Nezamzadeh-Ejhieh, M. Khorsandi, and J. Hazard. *Mater*, **176**(2010):629–637. DOI: https://doi.org/10.1016/j.jhazmat.2009.11.077.

[23] F.M. Sanakousara, C.C. Vidyasagara, S.S. Chigaria, V.M. Jiménez-Pérezb, C.C. Viswanathc, K. Prakashd, and M.B. Sridhara. *Iran. J. Catal*, **13**(2023):57–72. DOI: https://doi.org/10.30495/IJC.2023.1973011.1975.

[24] M. Rezaei and A. Nezamzadeh-Ejhieha. *Int. J. Hydrogen Energy*, **45**(2020):24749–24764. DOI: https://doi.org/10.1016/j.ijhydene.2020.06.258.

[25] M. Rezaei, A. Nezamzadeh-Ejhieh, and A.R. Massah. *Ecotoxicol. Environ. Saf*, **269**(2024):115927, . DOI: https://doi.org/10.1016/j.ecoenv.2024.115927.

[26] M. Rezaei, A. Nezamzadeh-Ejhieh, and A.R. Massah. *ACS Omega*, **9**(2024)(6):6093–6127, . DOI: https://doi.org/10.1021/acsomega.3c07560.

[27] Y. Niu, P. Huang, F. Li, K. Yang, J. Yang, R. Wang, C. Lin, and T. Qiu. *Int. J. Photoenergy*, **2016**(2016):1–12. DOI: https://doi.org/10.1155/2016/4618924.

[28] M.J. Borah, A. Devi, R.A. Saikia, and D. Deka. *Energy*, **158**(2018):881–889. DOI: https://doi.org/10.1016/j.energy.2018.06.079.

[29] M. Visa, L. Andronic, A. Duta, and J. Environ. *Manage*, **150** (2015):336–343, . DOI: https://doi.org/10.1016/j.jenvman.2014.10.026.

[30] M. Guo, W. Jiang, C. Chen, S. Qu, J. Lu, W. Yi, and J. Ding. *Energy Convers. Manag*, **229**(2021):113745. DOI: https://doi.org/10.1016/j.enconman.2020.113745.

[31] Z. Bi, X. Liu, Y. Zhang, Y. Zhang, Y. Ma, Y. Chen, J. Zhou, and S. Ruan. *Appl. Phys. Lett*, **124**(2024)(2):022101. DOI: https://doi.org/10.1063/5.0187144.

[32] D.T. Bekele, N.T. Shibeshi, and A.S. Reshad. *Bioenerg. Res*, **16** (2023):1361–1379. DOI: https://doi.org/10.1007/s12155-022-10546-7.

[33] D. Nunes, A. Pimentel, R. Branquinho, E. Fortunato, and R. Martins. *Catalysts*, **11**(2021):504. DOI: https://doi.org/10.3390/catal11040504.

[34] A. Khlyustova, N. Sirotkin, T. Kusova, A. Kraev, V. Titov, and A. Agafonov. *Mater. Adv*, **1**(2020)(5):525–553. DOI: https://doi.org/10.1039/D0MA00171F.

[35] J. Pang, J. Sun, M. Zheng, H. Li, Y. Wang, and T. Zhang. *Appl. Catal. B Environ*, **254**(2019):510–522. DOI: https://doi.org/10.1016/j.apcatb.2019.05.034.

[36] S.S. Alterary, N.H. Marei, and J. King Saud. *Univ. - Sci*, **33**(2021):101536. DOI: https://doi.org/10.1016/j.jksus.2021.101536.

[37] X. Li, J. Xiong, Z. Tang, W. He, Y. Wang, X. Wang, Z. Zhao, and Y. Wei. *Molecules*, **28**(2023):1653, . DOI: https://doi.org/10.3390/molecules28041653.

[38] J. Song, X. Wang, Y. Bu, J. Zhang, X. Wang, J. Huang, J. Chen, and J. Zhao. *Environ Sci Pollut Res*, **23** (2016):22793–22802. DOI: https://doi.org/10.1007/s11356-016-7353-2.

[39] S. Liu, J. Zhu, X. Guo, J. Ge, and H. Wu. *Colloids Surfaces A Physicochem. Eng. Asp*, **484**(2015):434–440, . DOI: https://doi.org/10.1016/j.colsurfa.2015.08.033.

[40] E. Soco, D. Papciak, and M.M. Michel. *Minerals*, **10**(2020):66. DOI: https://doi.org/10.3390/min10010066.

[41] Y. Yan, X. Zhou, J. Lan, Z. Li, T. Zheng, W. Cao, N. Zhu, W. Liu, and J. Photochem. *Photobiol. A Chem*, **367**(2018):355–364. DOI: https://doi.org/10.1016/j.jphotochem.2018.08.045.

[42] E. Mares, M.A. Gonçalves, P.T.S da Luz, G.N.D. Rocha Filho, J.R. Zamian, and L.R.V. da Conceicao. *Fuel*, **299**(2021):120887. DOI: https://doi.org/10.1016/j.fuel.2021.120887.

[43] L.L. Son, T.T. Van, K. Q. Trung, N.V. Hieu, D.D. Trung, and N.D. Cuong. *J. Electron. Mater*, **48**(2019):7897–7905. DOI: https://doi.org/10.1007/s11664-019-07616-6.

[44] M. Visa, M. Cosnita, M. Moldovan, C.A. Marin, and M. Mihaly. *Int. J. Environ. Res. Public Health*, **18**(2021):3887, . DOI: https://doi.org/10.3390/ijerph18083887.

[45] G. Li, Q. Teng, B. Sun, Z. Yang, S. Liu, and X. Zhu. *Colloids Surfaces A Physicochem. Eng. Asp*, **624**(2021):126795, . DOI: https://doi.org/10.1016/j.colsurfa.2021.126795.

[46] O.D. Okechukwu, E. Joseph, U.C. Nonso, and N.O. Kenechi. *Clean. Chem. Eng*, **3**(2022):100038. DOI: https://doi.org/10.1016/j.clce.2022.100038.

[47] J. Huang, Y. Jian, P. Zhu, O. Abdelaziz, and H. Li. *Front. Chem*, **10**(2022):1–7. DOI: https://doi.org/10.3389/fchem.2022.904251.

[48] M.K. Lam and K.T. Lee. *Fuel Process. Technol*, **92**(2011):1639–1645. DOI: https://doi.org/10.1016/j.fuproc.2011.04.012.

[49] N.S.A. Manab, H. Veny, A. Gusniah, S. Sulaiman, and N. Aziz. *ASEAN J. Chem. Eng*, **21**(2021):19–26. DOI: https://doi.org/journal.ugm.ac.id/v3/AJChE/article/view/9144.

[50] B. Liu, B. Yao, S. Gonzalez-Cortes, V.L. Kuznetsov, M. AlKinany, S.A. Aldrees, T. Xiao, and P.P. Edwards. *Appl Petrochem Res*, **7**(2017):55–66, . DOI: https://doi.org/10.1007/s13203-017-0178-1.

[51] N. Ghani, J. Iqbal, S. Sadaf, H. Nawaz Bhatti, and M. Asgher. *ChemistrySelect*, **5**(2020):9245–9253. DOI: https://doi.org/10.1002/slct.202001913.

[52] M. Gohain, K. Laskar, H. Phukon, U. Bora, D. Kalita, and D. Deka. *Waste Manag*, **102**(2020):212–221. DOI: https://doi.org/10.1016/j.wasman.2019.10.049.

[53] A.S. Redjeki, S. Sukirno, and S. Slamet. *Bull. Chem. React. Eng. Catal*, **16**(2021)(4):816–830. DOI: https://doi.org/10.9767/bcrec.16.4.11690.816-830.

[54] A. Gnanaprakasam, V.M. Sivakumar, A. Surendhar, M. Thirumarimurugan, and T. Kannadasan. *J. Energy*, **2013**(2013):1–10. DOI: https://doi.org/10.1155/2013/926392.

[55] U. Coleto Jr, R.A.C. Amoresi, V. Teodoro, I.M. Ianil, E. Longo, M.A. Zaghete, L.A. Perazolli, and J. Mater. *Sci. Mater. Electron*, **29**(2018)(23):20329–20338. DOI: https://doi.org/10.1007/s10854-018-0167-x.

[56] G. Corro, U. Pal, and N. Tellez. *Appl. Catal. B Environ*, **129**(2013):39–47, . DOI: https://doi.org/10.1016/j.apcatb.2012.09.004.